15TH IEA HEAT PUMP CONFERENCE
MAY 26–29, 2026 | HOFBURG
VIENNA 2026
DECARBONISATION THROUGH INNOVATION

Enhancing Performance of Large-Scale Heat Pumps: The Impact of Refrigerant Choices and Off-Design Operations in District Heating Systems

Sebastian Ostlender[a], Peter Noelke[a], Ben Spoek[a], Moritz Zuschlag[a], Jonas Klingebiel[a], Dirk Müller[a]

[a] RWTH Aachen University, Institute for Energy Efficient Buildings and Indoor Climate, Mathieustr. 10, Aachen, Germany

Abstract

Large-scale heat pumps (LSHPs) are a key technology for decarbonizing district heating systems. While simulation studies highlight their potential and optimization strategies, many simplify LSHP performance and neglect detailed refrigerant-cycle modeling, overlooking efficiency and heating capacity variations during off-design operation—when source or sink temperatures differ from the design point.
Off-design performance is strongly influenced by the refrigerant and cycle configuration. Considering these factors during system design can improve integration and efficiency in energy systems. Building on this, we analyze twelve refrigerant–flowsheet combinations in a district heating system to derive design recommendations for LSHP integration.
We compare R717, R600a, R246fa, and R1224yd(Z) with standard, internal-heat-exchanger, and vapor-injection cycles. Off-design efficiency and heating capacity are calculated using detailed Python-based component models that account for refrigerant effects and advanced compressor and heat exchanger models.
Annual simulations consider varying source and sink temperatures and interactions between system components, including LSHP, storage, heating rod, controller, and district heating network. The system's maximum heat demand is 1.3 MW, with sink temperatures ranging from 70 °C to 90 °C and source temperatures from 9 °C to 25 °C.
R717-LSHPs achieve, on average, 8% higher efficiency at the design point but also show greater reductions in heating capacity during off-design operation, increasing backup heater use by up to 6%. Depending on the backup system, this can influence the optimal refrigerant choice compared to neglecting off-design effects.
The study demonstrates that both COP and available heating capacity across operating conditions significantly affect energy hub efficiency. It highlights the need for detailed off-design refrigerant-cycle analysis to inform reliable LSHP design and integration in district heating networks.
© HPC2026.
Selection and/or peer-review under the responsibility of the organizers of the 15th IEA Heat Pump Conference 2026.

Keywords: Large-scale heat pumps; District heating networks; Off-design performance; Refrigerant-cycle modeling

1. Introduction

Germany's district heating systems are predominantly supplied by fossil fuel–based heat generation [1]. Simultaneously, the share of district heating in the overall heat supply is projected to increase substantially over the coming decades [2]. This trend highlights the urgent need for strategic measures, encompassing both the planning and implementation of new low-carbon district heating systems and the systematic decarbonization of existing systems, particularly the 2nd- and 3rd-generation of district heating systems, where supply temperatures typically range from approximately 90 °C (3rd generation) to 120 °C (2nd generation) [3].

In most energy transition scenarios, large-scale heat pumps (LSHPs) are considered a key technology for the sustainable transformation of district heating [4]. By 2045, a significant proportion of district heat — estimated at 41 % — is projected to be supplied by LSHPs [2]. However, the number of installed systems remains low, as technical and economic uncertainties continue to impede investments and large-scale deployment [4]. To address these challenges, an increasing number of simulation-based studies have investigated LSHP integration into district heating systems, focusing on heat source selection and optimal network integration.

1.1. Review of Large-Scale Heat Pumps in District Heating Networks

Lund et al. [5] analyzed LSHP integration in the Danish energy system, differentiating between district heating systems with and without combined heat and power (CHP) plants. This classification accounted for interactions with the electricity grid, enabling CHP-generated electricity to be used by LSHPs. The authors determined optimal LSHP capacities to minimize system costs under two price scenarios (2013 and 2025). Their results indicate that LSHP potential in Denmark could rise from 2.7 GW_{th} in 2013 to 4 GW_{th} in 2025, although this potential is highly sensitive to electricity and gas prices.

Averfalk et al. [6] summarized operational experiences of LSHPs coupled with CHP units in Swedish DHNs and analyzed the types of heat sources employed. Wastewater was identified as the most frequently used source, followed by surface water and industrial waste heat. The authors emphasized that future capacity allocation within combined systems will depend on electricity prices, availability of excess electricity, and CO_2 taxation.

Pieper et al. [7] conducted a case study in Tallinn, Estonia, evaluating 13 potential LSHP locations and different heat sources, including ambient air, flue gases, surface water, and geothermal energy. In the study, CHP units supply half of the heat demand, with gas boilers covering peak loads. The heat pump efficiency (COP – Coefficient of Performance) values were determined using a generic approximation based on source and sink temperatures, component characteristics, and refrigerant properties, with the system designed for the coldest winter day. The results indicate that LSHPs could meet 16% of Tallinn’s heat demand, and a system incorporating LSHPs was 27% more cost-effective than one relying solely on gas boilers. Significantly, LSHP capacity design was strongly influenced by both heat source selection and seasonal temperature variations.

Collectively, these studies demonstrate that LSHP deployment in DHSs is feasible and can provide a viable alternative to conventional fossil-fuel-based heating. Nevertheless, economic viability is highly sensitive to external factors, such as the electricity-to-gas price ratio, and component specific factors, including investment costs and COP during operation.

1.2. COP Modeling Approaches

For simulation studies, four main approaches are widely employed to model heat pump COP:

(1) **Constant COP models**, in which the COP is assumed to be independent of operating temperatures and load conditions.
(2) **Carnot- or Lorenz-based models**, in which COP is derived from theoretical efficiencies and scaled by a performance factor, accounting for source and sink temperatures.
(3) **Physics-based models**, capturing the detailed thermodynamic behaviour of the refrigerant cycle.
(4) **Data-based models** use measurement data to predict heat pump efficiency and heating capacity.

Model complexity increases from approach (1) to (3). **Constant COP** models are commonly applied in preliminary concept studies or large-scale energy system analyses [5], where detailed operational temperature data are unavailable. **Carnot- or Lorenz-based models** allow evaluation under varying temperature profiles, providing a more detailed assessment of system performance [8]. **Physics-based models** offer the highest level of detail, enabling simulation of off-design operation and capturing the influence of component selection, cycle design, and refrigerant choice. Consequently, these models are particularly suitable for plant-specific performance analysis and detailed optimization. **Data-based models** require large amounts of measurement data and can accurately reproduce the behavior of a specific heat pump. However, their interpretability is limited, and the transferability of the trained models to other heat pump configurations is generally restricted.

Pieper et al. [9] compared four models across the categories (1) to (3) in a case study on LSHP source selection in Denmark. Both source and sink temperatures fluctuated throughout the year. A physics-based model of a two-stage R717 LSHP, designed for the coldest day, served as the reference. The study showed substantial deviations in COP (up to 60%) depending on the model and heat source. Subsequent economic analysis revealed that heat source selection is strongly influenced by the modeling approach.

Experimental and simulation-based studies further indicate that COP and volumetric heating capacity (VHC) are affected not only by source and sink temperatures but also by refrigerant choice, flowsheet option, and the cycle components (compressor, heat exchanger, etc.) itself [10-14]. Different refrigerant–refrigerant-flowsheet combinations dominate performance in different temperature ranges. Strong temperature dependence of VHC can necessitate auxiliary heating to meet demand, potentially reducing overall COP advantages if the auxiliary heater operates at low efficiency. Comparative studies typically evaluate COP and VHCseparately, highlighting the need for a multidimensional assessment when designing LSHPs for district heating systems [15].

1.3. Research Gap and Study Objective

To summarize the current state of research, LSHPs are increasingly recognized as crucial for decarbonization of district heating systems. For initial studies [5, 6] , simplified heat pump models (Constant or Carnot based) and are often employed. However, these approaches do not capture key influences of the refrigerant cycle on COP and VHC and therefore cannot fully represent the performance-relevant behaviour of the system. However, comparative studies already indicate that these effects have a direct impact on design-relevant decisions [9]. So far, the comparisons have focused primarily on the differences between the individual modelling approaches (1) to (3). A comprehensive comparison across multiple refrigerants and flowsheet options is currently lacking.

To address this gap, the present study compares four refrigerants across three flowsheet configurations in a LSHP for an energy hub, with a focus on overall district heating system performance. In addition, a simplified Carnot-based model is included as a reference. An exemplary use case is employed to facilitate the comparison.

Section 2 introduces the use case and the modeling approaches for both the LSHP and the overall system, including the backup heater, storage, controller, and district heating network. Section 3 presents simulation results for the considered refrigerant–flowsheet combinations. Finally, section 4 discusses the findings and outlines potential directions for further development.

2. Use Case and Modelling Approach

The use case consists of a district heating network (DHN), representing the piping system and heat demand of all connected buildings, as well as an energy hub. The total heat demand of the DHN is generated using the District Generator [16] for a representative district, as defined in bey Benthin et al. [17] (example 1). The district comprises 40 buildings of various types, including both space heating and domestic hot water demands. For parameterization, building data from the TABULA project [18] and the German Environment Agency [19] are used. Hourly heat demand is calculated based on weather data from the German Weather Service (DWD) [20].

The heat demand, as well as the supply temperatures of the DHN are shown in Figure 1. The peak heat demand reaches $1.3\ MW$. The supply temperature of the DHN is defined by an outdoor-temperature-dependent heating curve [21]. Sewage water is used as the heat source, providing temperatures above 9 °C throughout the year [22].

Based on VDI 4646 [23], four refrigerants are selected for the temperature range from 10 °C source to 90 °C sink (see Table 1). Both natural and synthetic refrigerants are considered. Three flowsheet options are evaluated (see Figure 2): the standard cycle, a cycle with an internal heat exchanger (IHX), and a cycle with flash injection into the compressor (VI). Compared to the standard cycle, the IHX cycle allows higher evaporation pressure and provides the required superheating within the IHX. The VI cycle achieves higher specific heating capacities and reduces expansion losses, particularly at high temperature lifts. [24]

The system modeling is conducted in two steps. The first step (Subsection 2.1) focuses on generating performance maps for each refrigerant–cycle combination. The second step (Subsection 2.2) involves integrating these performance maps into a system model for annual simulations of the district heating system.

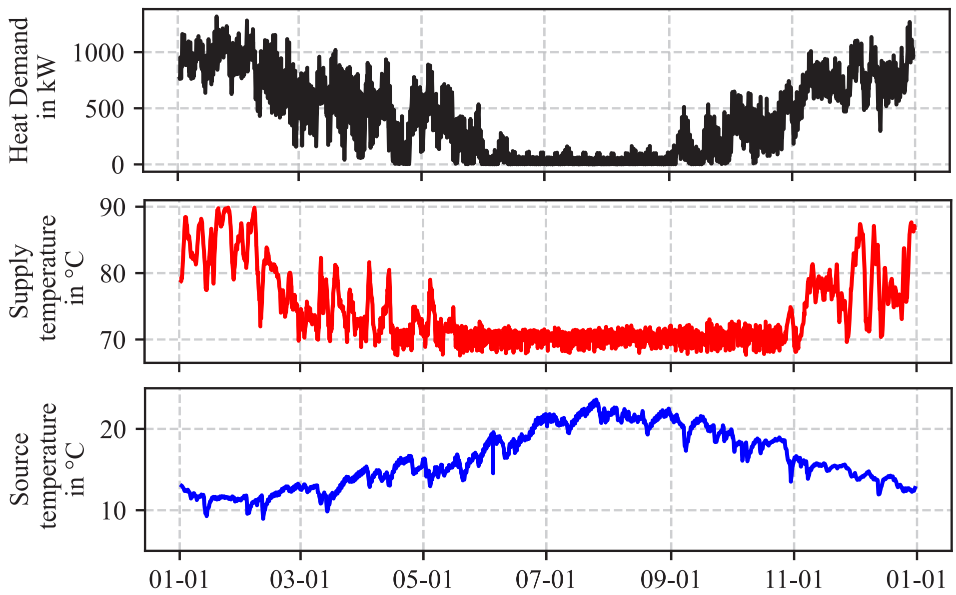

Figure 1: Annual profiles of heat demand, supply temperature, and source temperature of the LSHP in this study.

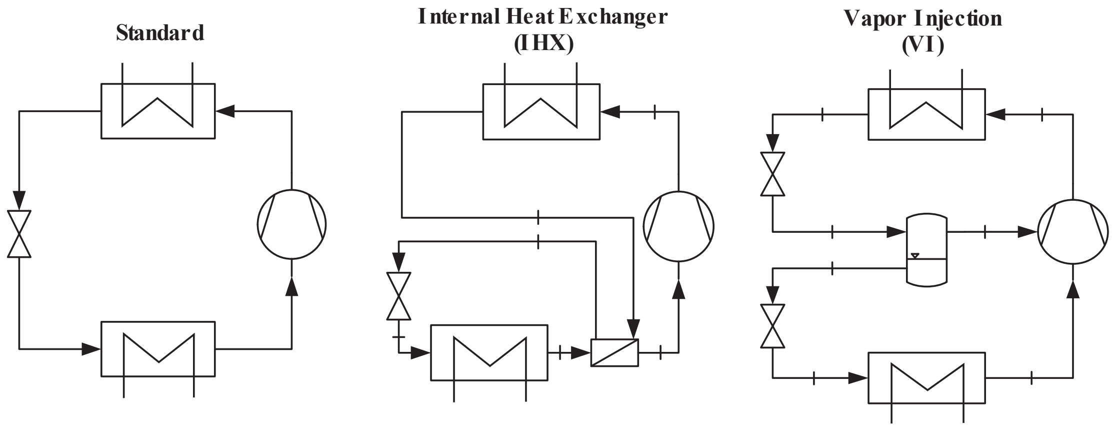

Figure 2: Flowsheets investigated in this study

2.1. Refrigerant Cycle Modelling

Performance maps are generated for all refrigerant–flowsheets combinations, capturing both COP and heating capacity across the full range of operating points. Each operating point is defined by the secondary inlet conditions (temperature and mass flow rate) at the evaporator and condenser, as well as the compressor speed. COP and heat heating capacity are calculated using an iterative algorithm that solves the thermodynamic states throughout the refrigerant cycle. This approach is implemented using the open-source Python package VCLibPy [25].

The package includes a semi-physical compressor model based on [26], while heat exchangers are modeled using a moving boundary approach that divides the heat transfer process into distinct regimes: subcooled, two-phase, and superheated. For each regime, heat transfer is calculated using the ε–NTU method with constant overall heat transfer coefficients based on [27]. Pressure losses within components are neglected, and the dependency of performance on compressor speed is not considered. Furthermore, a constant degree of superheating of $5\,K$ and subcooling of $3\,K$ is assumed across all operating points.

For each refrigerant–flowsheet combination, the component dimensions are optimized to maximize the COP at the design point and achieve a nominal heating capacity of $780\ kW$, corresponding to $60\ \%$ of the peak load, as recommended in planning guidelines [21]. According to VDI 4646, the design point is defined as the operating condition at which the heat pump operates most frequently (W15W77), excluding summer operation. Component design includes the heat exchanger surface areas and the compressor displacement volume. The design procedure follows the cycle calculation approach described in [28], in which a minimum temperature difference between the refrigerant and the secondary fluid is imposed for all heat exchangers. This minimum temperature difference is set to $5\ K$ for all configurations.

2.2. Dynamic Simulation Model of the District Heating System

The performance maps described in Section 2.1 are used to integrate the heat pump characteristics into annual simulations of the district heating system. The system model consists, in simplified form, of two main subsystems: the district heating network (DHN), which represents the heat demand, and the energy hub, which supplies the required thermal energy. All components are implemented in Modelica.

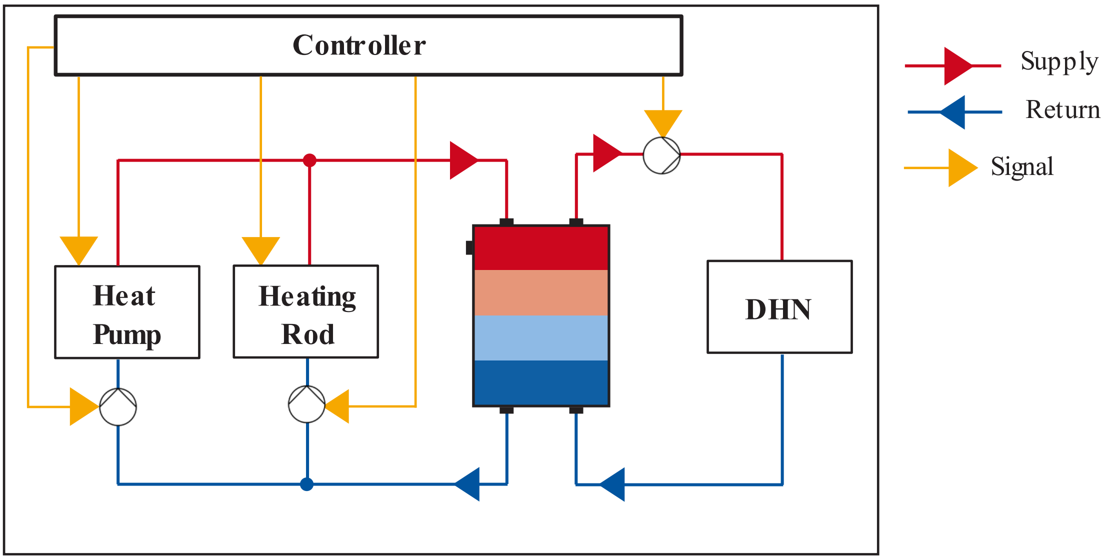

Figure 3: Configuration of the system model consisting of a heat pump, heating rod, thermal storage, controller, and district heating network (DHN)

The DHN is modeled in a simplified manner. The heat demand is integrated into the model via a time series. The network itself is represented as a thermal volume with inertia, from which heat is drawn to meet the demand, causing the supply temperature to cool down to the return temperature. The mass flow rate within the network is regulated to maintain a constant return temperature of $40\ °C$. During summer operation, a minimum mass flow rate is enforced to ensure hydraulic stability, resulting in elevated return temperatures.

The energy hub consists of a buffer storage, a LSHP, an heating rod, and a system controller. The buffer storage model is based on the AixLib [29] buffer storage model, which features three vertical layers and accounts for both convective and diffusive heat transfer between layers. The total storage capacity is $1000\ kWh$, corresponding to a temperature difference of $45\ K$.

The heating rod is modeled with a constant efficiency of 98 %. Its heating capacity is set to $520\ kW$, allowing the LSHP and the heating rod together to meet the peak demand of $1.3\ MW$. The LSHP can be represented either by the performance maps developed in Section 2.1 or by an idealized Carnot-based approach. In the latter case, the COP is calculated based on the Carnot-COP and an efficiency factor η_{Carnot} of $50\ \%$, using the evaporator inlet temperature as the heat source temperature and the condenser outlet temperature as the heat sink temperature (Eq. 1). As with the detailed models, the design capacity is set to 780 kW. For the Carnot-based model, this capacity also represents the maximum output, which—unlike the detailed models—is independent of external factors such as source and sink temperatures.

$$COP = \frac{1}{1-\frac{\mathrm{T_{source}}}{\mathrm{T_{sink}}}} \cdot \eta_{\mathrm{Carnot}} \tag{1}$$

The system control is implemented using proportional–integral (PI) controllers. A central PI controller adjusts the heat pump compressor speed and the relative power of the electric heater to maintain the temperature of the upper storage layer according to the heating curve. The heat pump is used as the primary heat generator, with the electric heater activated as needed. Additional PI controllers regulate the mass flow rates of the individual heat generators to achieve their respective outlet temperatures. Each generator charges the storage with a temperature offset of +1 K above the set supply temperature to ensure stable operation and maintain stratification.

Table 1: Refrigerants Investigated in this study and system configuration

Refrigerant and Classification		System Configuration		
R717	Natural	Peak Demand	$\dot{Q}_{\mathrm{DHN}}$	1300 kW
R600a	Natural (HC)	Nominal Capacity LSHP	$\dot{Q}_{\mathrm{nom,LSHP}}$	780 kW
R1224yd(Z)	HCFO	Nominal Capacity Heating Rod	$\dot{Q}_{\mathrm{nom,HR}}$	520 kW
R236fa	HFC	Storage Capacity	Q_{Storage}	1000 kWh

3. Results

The investigations are structured into two parts. First, the performance maps of the refrigerant–flowsheet combinations are analyzed. In the second part, annual simulations are conducted to evaluate the performance of these combinations within a district heating system.

3.1. Refrigerant – Flowsheet Comparison

Figure 4 illustrates the twelve refrigerant–cycle combinations investigated at three operating points: the point with the largest temperature lift (W9W90), the point with the smallest temperature lift (W24W70), and the design point (W15W77). At all operating points, the condenser inlet temperature is held constant at 40 °C, since the DHN return temperature is held constant. The temperature difference across the evaporator is constant at 3 K. The comparison considers both the COP and the heating capacity $\dot{Q}_{\mathrm{th,LSHP}}$.

At the design point, the heating capacities are, by definition, identical across all configurations (see Figure 4e). However, differences in COP are evident. In general, the highest COP values are obtained when using R717 as the refrigerant and the IHX flowsheet configuration. Accordingly, the maximum COP of 3.26 is achieved with the combination of R717 and the IHX flowsheet at the design point (see Figure 4b). In contrast, the lowest COP of 2.10 is observed for the R236fa–standard cycle configuration.

At the other operating points, the combination of R717 with the IHX flowsheet continues to dominate the COP comparison. However, the differences between individual cycle configurations depend on the operating point. For instance, the COP of the R600a-standard cycle is higher than that of the R1224yd(Z)–standard cycle at W9W90 (Figure 4a), whereas at W24W70 (Figure 4c) the R1224yd(Z)–standard cycle exhibits a higher COP. The same trend applies to the R600a–IHX and R1224yd(Z)–IHX combinations. At W9W90, the COP differences between the IHX and VI cycle configurations are smaller than at the other operating points; in some cases, the ranking even reverses, and the VI cycle achieves a higher COP than the IHX cycle. The VI cycle reduces throttling losses by separating the vapor and liquid phases at an intermediate pressure level. Since expansion losses increase with larger temperature lifts, this advantage of the VI cycle becomes more significant under high-lift conditions, allowing it to outperform the IHX flowsheet.

Outside the design point, differences in heating capacities between the cycle variants are also observed. At W9W90 (Figure 4d), R717-based combinations reach the highest heating capacities, up to 90% of the nominal design capacity, whereas the R236fa–IHX cycle drops to around 60% $(465\ kW)$. At W24W70 (Figure 4f), the R600a–IHX combination achieves the highest capacity, reaching $128\ \%$ $(1000\ kW)$ of the nominal design capacity. These results further highlight the complex interactions between refrigerants and flowsheet configurations.

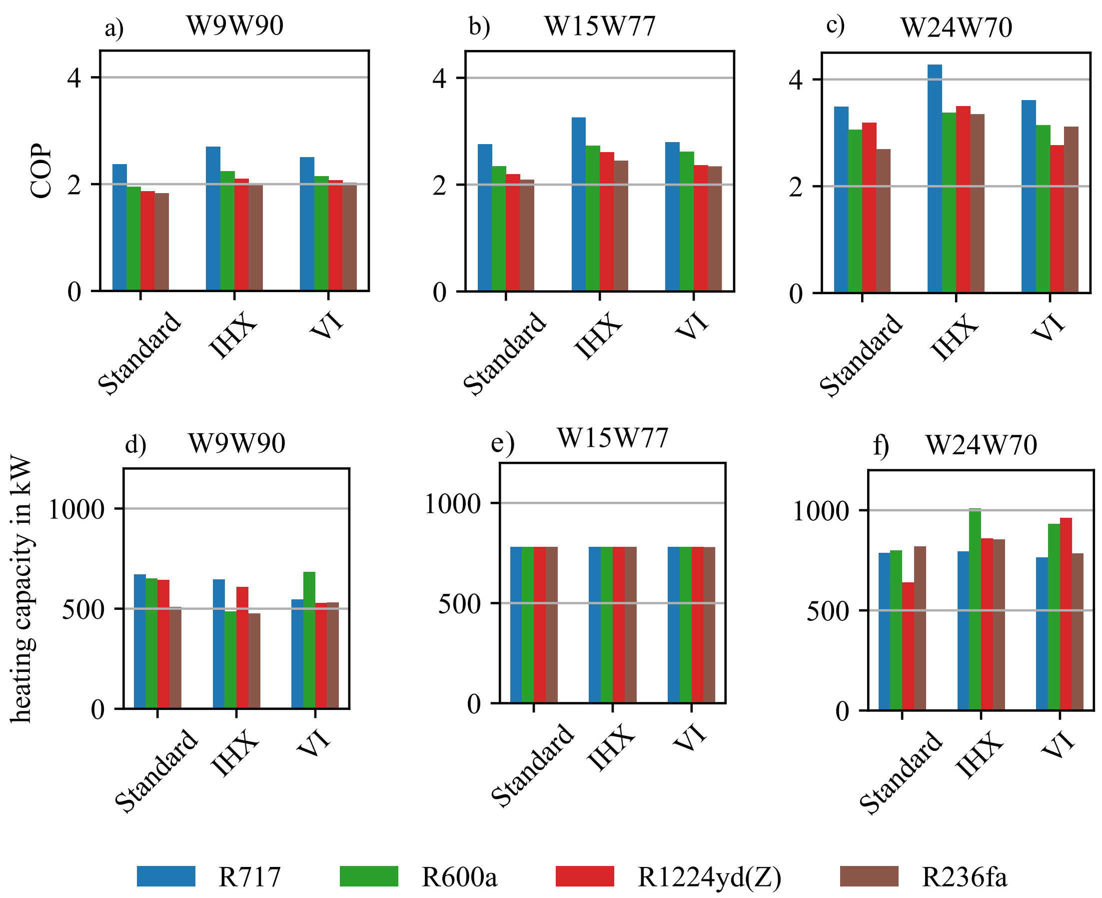

Figure 4: Comparison of refrigerants and cycles at three operating points: maximum lift (W9W90), design point (W15W77), and minimum lift (W24W70). COP (a-c) and heating capacity (d-f) at maximum compressor speed are compared.

3.2. Annual System Simulations

The impact of differences in heating capacity and efficiency on annual system performance is investigated in the following section. For clarity, only selected cycle configuration models (four refrigerant-dependent and the Carnot model) are considered initially.

Figure 5 illustrates an exemplary operation week (January 18–24) characterized by high heat demands of the district heating network, reaching up to $1250\ kW$, accompanied by increasing supply temperatures from $80\ °C$ to $90\ °C$ due to lower ambient temperatures. The source temperature fluctuates between $11\ °C$ and $12\ °C$, remaining below the design temperature of $15\ °C$.

The operation conditions are identical across all cycle configuration models; however, the available heating capacities of the heat pumps differ. While the Carnot-based model continuously provides the nominal heating capacity of $780\ kW$, the other cycle configuration models deliver up to $130\ kW$ less ($-16\ \%$), requiring additional operation of the electric heater to meet the demand. For all refrigerant-dependent configurations, the available heating capacity decreases with increasing sink temperature from $80\ °C$ to $90\ °C$. The largest reduction of $40\ kW$ is observed for the R236fa–IHX, consistent with the findings discussed in Section 3.1.

Furthermore, the COP varies notably across all model approaches. The highest COP is obtained with the refrigerant-dependent model of the R717–VI configuration, reaching values of up to 2.5, while the lowest COPs are observed for the R236fa–IHX and R600a–standard configurations, both around 2.0. The simplified Carnot-based model yields a COP of approximately 2.3, the second highest. However, compared to the R717–VI configuration, it exhibits a stronger dependency on the supply temperature.

The combined effect of COP and available heating capacity becomes evident when analyzing the energy hub's electricity consumption. The Carnot model and the R717–VI configuration exhibit the lowest electricity consumption. In contrast, the other configurations show an approximately 7% higher electricity consumption. A particularly noteworthy comparison arises between the R1224yd(Z)–IHX and R236fa–IHX configurations. Although R1224yd(Z)–IHX achieves higher COP values, its lower heating capacity offsets this advantage, resulting in nearly identical electricity consumption for both configurations over the analyzed period.

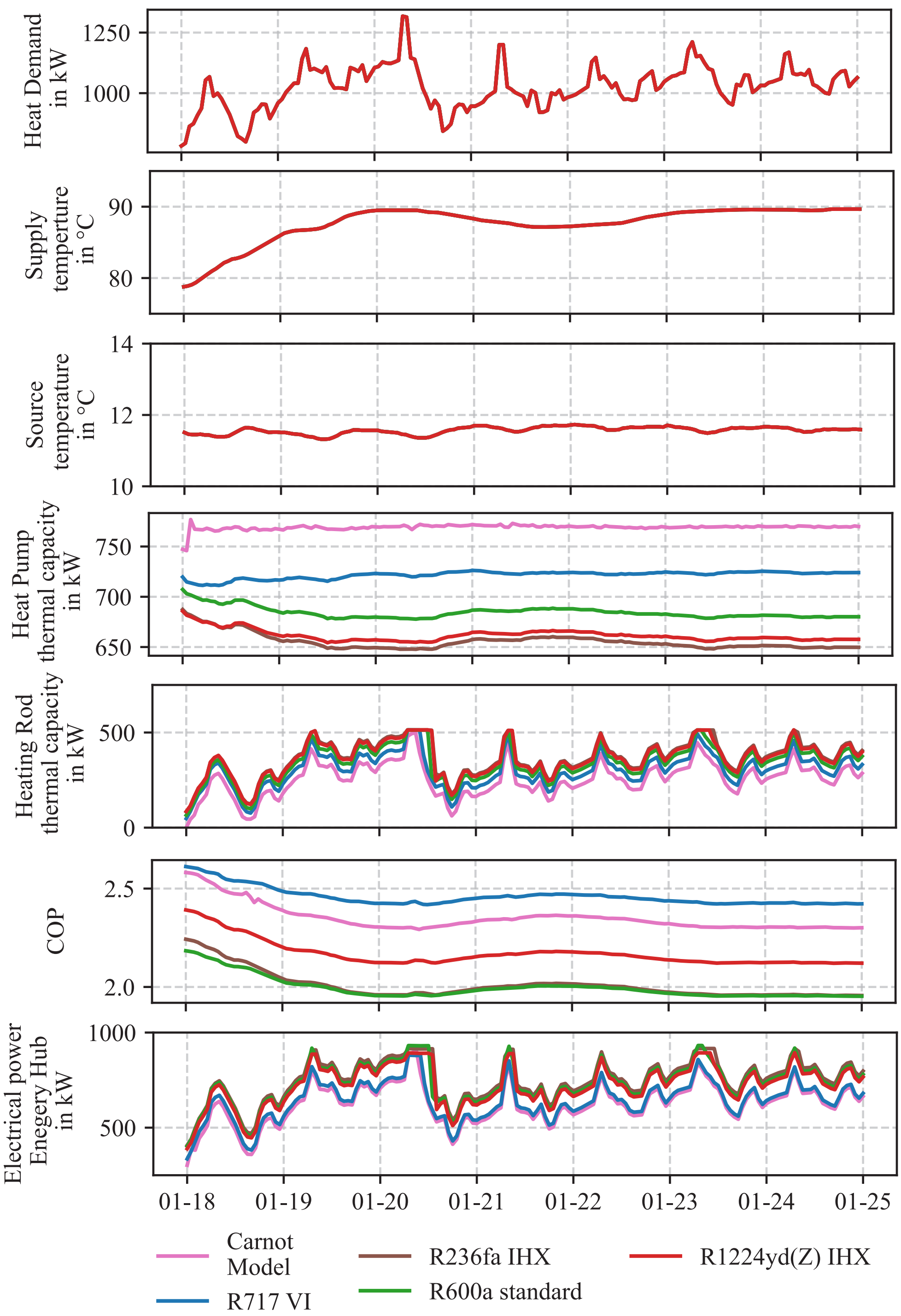

Figure 5: Comparison of operational characteristics of four refrigerant-based models and the Carnot model under dynamic boundary conditions during a winter week (January 18–25)

The comparison of the cycle models during the winter week reveals that, in addition to the COP, the available heating capacity outside the design point constitutes a relevant design criterion. Reduced heating capacities must be compensated by increased operation of auxiliary heaters, which can significantly decrease the overall system efficiency.

Figure 6 illustrates an additional representative week (April 06-11) during the transitional season characterized by moderate heat demands. Compared to winter operation, stronger fluctuations in heat demand occur due to a higher relative share of domestic hot water demand, which is concentrated over a few hours per day. During this period, the total heat demand ranges from $240\,kW$ to $740\,kW$ and can be fully supplied by the heat pump.

The PID controller adjusts the relative compressor speed, reducing it during periods of lower demand. The compressor speeds of the Carnot-based heat pump model are slightly higher than those of the refrigerant-dependent models. This behavior can be attributed to the higher available heating capacity at lower temperature lifts (see Section 3.1), which allows the Carnot-based model to meet the same thermal load at relatively lower part-load ratios.

Figure 7 presents the annual integrated values for the relative heat share of the heat pump, x_{LSHP} (Eq. 2), which relates the heat produced by the LSHP Q_{LSHP} to the total heat demand Q_{Demand}. In addition, the seasonal coefficient of performance of the entire energy hub, $SCOP_{\mathrm{EH}}$, is shown. This metric expresses the total heat demand relative to the total electrical energy input required by both the LSHP ($W_{\mathrm{el,LSHP}}$) and the heating rod $W_{\mathrm{el,HR}}$ (Eq. 3).

$$x_{\mathrm{LSHP}} = \frac{Q_{\mathrm{LSHP}}}{Q_{\mathrm{DHN}}} \tag{2}$$

$$SCOP_{\mathrm{EH}} = \frac{Q_{\mathrm{DHN}}}{W_{\mathrm{el,LSHP}} + W_{\mathrm{el,HR}}} \tag{3}$$

Although x_{LSHP} for the R717–VI configuration is 2 %-points lower than that of the Carnot model—requiring slightly increased use of the heating rod—the $SCOP_{\mathrm{EH}}$ is still 5 %-points higher for R717–VI. Due to its higher COP, the configuration fully compensates for the additional electricity demand of the heating rod. A comparison between R600a–Standard and R1224yd(Z)–IHX further illustrates that, despite the higher share of heat supplied by the heat pump in R600a–Standard, the SCOP of the entire energy hub is higher for R1224yd(Z)–IHX. This is due to the approximately 10 % higher operational COP of R1224yd(Z)–IHX. However, the SCOP advantage of the overall energy hub is only around 6 %, as part of this efficiency gain is offset by the increased electricity consumption of the heating rod.

Overall, the heat pump's COP is the dominant factor influencing the $SCOP$ of the energy hub. Differences between the model approaches in terms of x_{LSHP} are limited to a maximum of 6 %-points, whereas variations in overall system efficiency reach up to 34 %-points.

The comparison of all cycle models is presented in Figure 8, showing the SCOP of the energy and the heat pump's full-load hours τ_LSHP. The full-load hours relate the total heat output of the heat pump Q_LSHP to its nominal design capacity Q ̇_(nom,LSHP) (Eq. 4). Although the design capacities are identical, the full-load hours differ due to variations in off-design performance among the individual refrigerant–flowsheets combinations. The highest full-load hours are observed for the Carnot-based model. In contrast, the detailed refrigerant-dependent models exhibit 100-200 fewer full-load hours. Regarding system efficiency, the R717 configurations dominate, while the R236fa configurations show the lowest efficiency. In general, the number of full-load hours is strongly influenced by the flowsheet: the highest values are achieved with the VI flowsheet (4125h-4150h), whereas the IHX combinations result in the lowest full-load hours (4040 - 4060), necessitating more frequent operation of the electric heater. Overall, this effect reduces the efficiency differences between cycle variants compared to the COP differences observed at the design point.

$$\tau_{\mathrm{LSHP}} = \frac{Q_{\mathrm{LSHP}}}{\dot{Q}_{\mathrm{nom,LSHP}}} \tag{4}$$

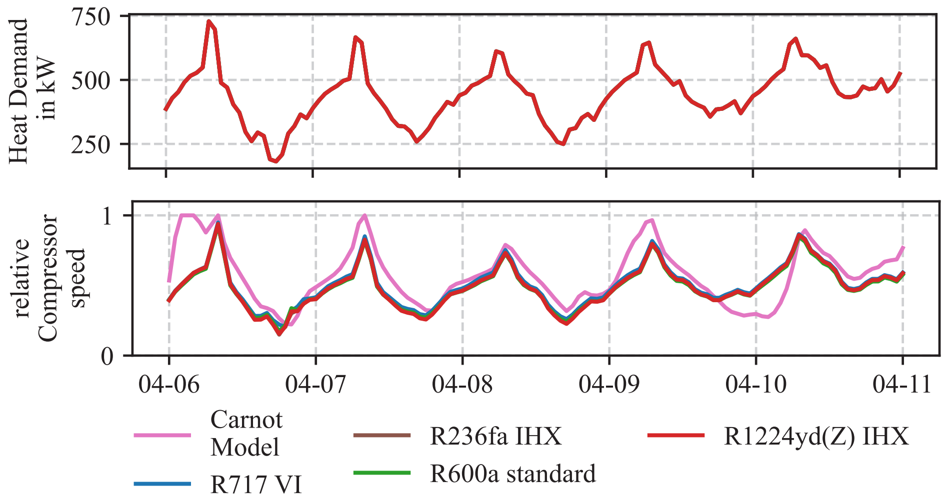

Figure 6:Comparison of operational characteristics of four refrigerant-based models and the Carnot model under dynamic boundary conditions during a week with moderate loads (April 6–11)

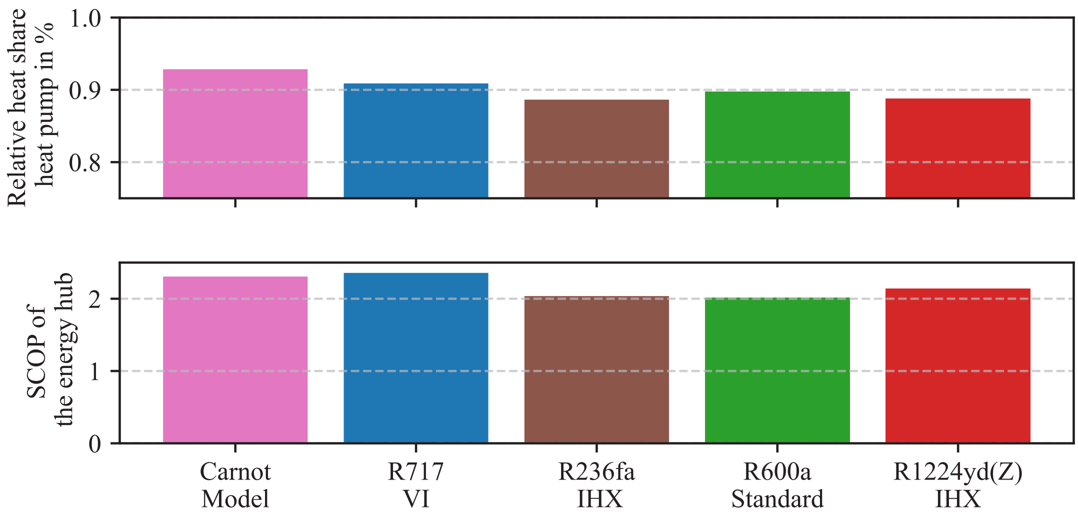

Figure 7: Comparison of heat supply by the heat pump and system efficiency for four refrigerant-based models and the Carnot model.

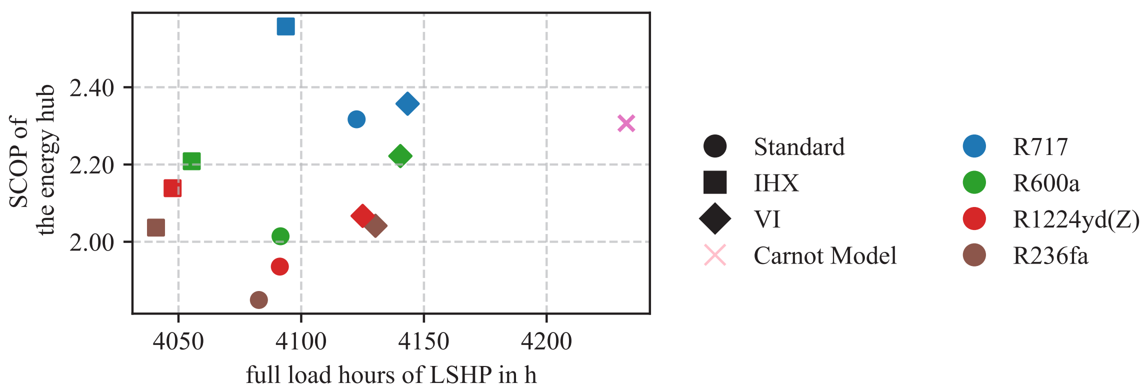

Figure 8: SCOP of the Energy Hub over the full load hours of the LSHP

4. Discussion and Conclusion

The present study is based on quasi-stationary calculations of the refrigerant–flowsheet combinations, combined with dynamic simulations in Modelica. So far, the influence of compressor speed on the compressor efficiency—and thus on COP and heating capacity—has been neglected. However, during summer operation, the heat pump also operates under partial load, which may lead to additional differences in overall system efficiency. For further investigations, it is therefore necessary to extend existing compressor models to account for speed dependency. Speed-dependent compressor models are often developed for specific compressor types and with a limited selection of refrigerants. According to Neumaier et al. [12], the choice of refrigerant has a significant impact on compressor efficiency, which must be considered when developing suitable models.

The dynamic simulations allow the influence of variable temperatures and system inertia on overall efficiency to be considered. Currently, the district heating network is represented in a simplified manner, for example by assuming a constant return temperature. In reality, the return temperature results from the supply-return-temperature difference of all building substations, which can vary depending on demand, mass flow, and potential faults [30]. Consequently, variations in the return temperature at the energy hub are also possible, which in turn affect the operating range of the heat pump. The specific impact of return temperature variations on overall system performance should therefore be investigated. The models presented in this study provide a suitable basis for such analyses.

This study presents a simulation-based investigation of twelve refrigerant–flowsheet combinations across the full operating range for use in a third-generation district heating system with sewage water as the heat source. In addition, a commonly used Carnot-COP model is included as a reference. Outside the design point, the refrigerant–flowsheet combinations differ not only in COP but also in available heating capacity, with variations of up to 13 %, whereas the heat capacity of the Carnot model remains constant across all operating points.

Annual simulations demonstrate that both COP and available heating capacity significantly affect the overall system efficiency ($SCOP_{EH}$) of the district heating system. COP advantages can be mitigated—or in some cases overcompensated—by limitations in available heating capacity and a higher use of an additional heater. Accordingly, evaluating the COP at a single operating point is insufficient for making informed design decisions between refrigerant and flowsheet variants. Such decisions should consider the demand profiles and the temperature levels during operation, particularly when COP differences between two options are small.

Through model enhancements and further studies, effects such as the influence of compressor efficiency or return temperature can be better understood. This enables the simulation-based investigation of complex interactions of LSHPs in district heating systems, providing a sound basis for informed design decisions.

References

[1] Prognos, Öko-Institut, Wuppertal-Institut, „Klimaneutrales Deutschland 2045. Wie Deutschland seine Klimaziele schon vor 2050 erreichen kann Langfassung im Auftrag von Stiftung Klimaneutralität, Agora Energiewende und Agora Verkehrswende“, 2021.

[2] Agora Energiewende und Prognos, GEF (2024), „Wärmenetze – klimaneutral, wirtschaftlich und bezahlbar. Wie kann ein zukunftssicherer Business Case aussehen?“ Zugegriffen: 10. November 2025. [Online]. Verfügbar unter: https://www.agora-energiewende.de/fileadmin/Projekte/2023/2023-18_DE_Business_Case_Waermenetze/A-EW_335_Businesscase_Waermenetze_WEB.pdf

[3] Y. Gong, G. Ma, Y. Jiang, und L. Wang, „Research progress on the fifth-generation district heating system based on heat pump technology“, *J. Build. Eng.*, Bd. 71, S. 106533, Juli 2023, doi: 10.1016/j.jobe.2023.106533.

[4] Agora Energiewende, Fraunhofer IEG, „Roll-out von Großwärmepumpen in Deutschland. Strategien für den Markthochlauf in Wärmenetzen und Industrie.“, 2023, *Fraunhofer-Gesellschaft*. doi: 10.24406/PUBLICA-1440.

[5] R. Lund, D. D. Ilic, und L. Trygg, „Socioeconomic potential for introducing large-scale heat pumps in district heating in Denmark“, *J. Clean. Prod.*, Bd. 139, S. 219–229, Dez. 2016, doi: 10.1016/j.jclepro.2016.07.135.

[6] H. Averfalk, P. Ingvarsson, U. Persson, M. Gong, und S. Werner, „Large heat pumps in Swedish district heating systems“, *Renew. Sustain. Energy Rev.*, Bd. 79, S. 1275–1284, Nov. 2017, doi: 10.1016/j.rser.2017.05.135.

[7] H. Pieper, V. Mašatin, A. Volkova, T. Ommen, B. Elmegaard, und W. Brix Markussen, „Modelling framework for integration of large-scale heat pumps in district heating using low-temperature heat sources“, *Int. J. Sustain. Energy Plan. Manag.*, S. Vol 20 (2019), März 2019, doi: 10.5278/IJSEPM.2019.20.6.

[8] P. A. Østergaard und A. N. Andersen, „Booster heat pumps and central heat pumps in district heating“, *Appl. Energy*, Bd. 184, S. 1374–1388, Dez. 2016, doi: 10.1016/j.apenergy.2016.02.144.

[9] H. Pieper, T. Ommen, J. Kjær Jensen, B. Elmegaard, und W. Brix Markussen, „Comparison of COP estimation methods for large-scale heat pumps used in energy planning“, *Energy*, Bd. 205, S. 117994, Aug. 2020, doi: 10.1016/j.energy.2020.117994.

[10] C. Höges, D. Roskosch, J. Brach, C. Vering, V. Venzik, und D. Müller, „Investigation of the Interactions between Refrigerant, Flowsheet, and Compressor in Residential Heat Pumps“, *Energy Technol.*, Bd. 11, Nr. 2, S. 2201295, Feb. 2023, doi: 10.1002/ente.202201295.

[11] C. Höges, V. Venzik, C. Vering, und D. Müller, „Bewertung alternativer Arbeitsmittel für Wärmepumpen im Gebäudesektor“, *Forsch. Im Ingenieurwesen*, Bd. 86, Nr. 2, S. 213–224, Juni 2022, doi: 10.1007/s10010-022-00584-0.

[12] L. Neumaier, D. Roskosch, J. Schilling, G. Bauer, J. Gross, und A. Bardow, „Refrigerant Selection for Heat Pumps: The Compressor Makes the Difference“, *Energy Technol.*, Bd. 11, Nr. 4, S. 2201403, Apr. 2023, doi: 10.1002/ente.202201403.

[13] P. Wang *u. a.*, „District heating utilizing waste heat of a data center: High-temperature heat pumps“, *Energy Build.*, Bd. 315, S. 114327, Juli 2024, doi: 10.1016/j.enbuild.2024.114327.

[14] C. Mateu-Royo, S. Sawalha, A. Mota-Babiloni, und J. Navarro-Esbrí, „High temperature heat pump integration into district heating network“, *Energy Convers. Manag.*, Bd. 210, S. 112719, Apr. 2020, doi: 10.1016/j.enconman.2020.112719.

[15] C. Mateu-Royo, C. Arpagaus, A. Mota-Babiloni, J. Navarro-Esbrí, und S. S. Bertsch, „Advanced high temperature heat pump configurations using low GWP refrigerants for industrial waste heat recovery: A comprehensive study“, *Energy Convers. Manag.*, Bd. 229, S. 113752, Feb. 2021, doi: 10.1016/j.enconman.2020.113752.

[16] S. Henn, J. D. Schölzel, T. Beckhölter, C. Wüller, R. Hamze, und D. Müller, „Districtgenerator: Generating building-specific load profiles for residential districts.“, *J. Open Source Softw.*, Bd. 10, Nr. 111, S. 7657, Juli 2025, doi: 10.21105/joss.07657.

[17] J. Benthin *u. a.*, „Integrierte Betrachtung von Strom-, Gas- und Wärmesystemen zur modellbasierten Optimierung des Energieausgleichs- und Transportbedarfs innerhalb der deutschen Energienetze. Gemeinsamer Abschlussbericht“. Zugegriffen: 17. November 2025. [Online]. Verfügbar unter: https://publica.fraunhofer.de/bitstreams/1ee9677a-2c3c-433f-959f-700ed429b44b/download

[18] „TABULA WebTool“. Zugegriffen: 17. November 2025. [Online]. Verfügbar unter: https://webtool.building-typology.eu/#bm

[19] „Wohnen und Sanieren Empirische Wohngebäudedaten seit 2002“. Zugegriffen: 17. November 2025. [Online]. Verfügbar unter: ttps://www.umweltbundesamt.de/sites/default/files/medien/1410/ publikationen/2019-06-03-barrierefrei-broschuere_wohnenundsanieren.pdf

[20] „Wetter und Klima - Deutscher Wetterdienst - Homepage“. Zugegriffen: 17. November 2025. [Online]. Verfügbar unter: https://www.dwd.de/EN/Home/home_node.html

[21] QM Fernwärme, Hrsg., *Planungshandbuch Fernwärme*, Version 1.2. Ittigen: EnergieSchweiz, Bundesamt für Energie BFE, 26.

[22] S. Ostlender, R. Kannengießer, P. Kröning, C. Vering, und D. Müller, „The Agony of the Choice in District Heating: The Impact of Heat Source for Heat Pumps“, 2023, doi: 10.23697/0REX-EF58.

[23] *VDI 4646 - Anwendung von Großwärmepumpen*. 2024. Zugegriffen: 20. Juli 2025. [Online]. Verfügbar unter: https://www.vdi.de/richtlinien/details/vdi-4646-anwendung-von-grosswaermepumpen

[24] C. Höges, V. Venzik, C. Vering, und D. Müller, „Decarbonizing Steam Generation with High Temperature Heat Pumps: Refrigerant Selection and Flowsheet Evaluation“.

[25] *RWTH-EBC/vclibpy*. (25. August 2025). Python. RWTH Aachen University - E.ON Energy Research Center - Institute for Energy Efficient Buildings and Indoor Climate. Zugegriffen: 17. November 2025. [Online]. Verfügbar unter: https://github.com/RWTH-EBC/vclibpy

[26] C. Mateu-Royo, J. Navarro-Esbrí, A. Mota-Babiloni, M. Amat-Albuixech, und F. Molés, „Thermodynamic analysis of low GWP alternatives to HFC-245fa in high-temperature heat pumps: HCFO-1224yd(Z), HCFO-1233zd(E) and HFO-1336mzz(Z)“, *Appl. Therm. Eng.*, Bd. 152, S. 762–777, Apr. 2019, doi: 10.1016/j.applthermaleng.2019.02.047.

[27] B. Zühlsdorf, W. Meesenburg, T. S. Ommen, J. E. Thorsen, W. B. Markussen, und B. Elmegaard, „Improving the performance of booster heat pumps using zeotropic mixtures“, *Energy*, Bd. 154, S. 390–402, Juli 2018, doi: 10.1016/j.energy.2018.04.137.

[28] Ostlender, S., Höges, C., Vering, C., und Müller, D., „Under variable conditions: Investigating the off-design performance of natural refrigerants in heat pumps.“, 16th IIR-Gustav Lorentzen Conference on Natural Refrigerants (GL2024). Proceedings. University of Maryland, College Park, Maryland, USA, August 11-14 2024. Zugegriffen: 17. November 2025. [Online]. Verfügbar unter: https://iifiir.org/en/fridoc/under-variable-conditions-investigating-the-off-design-performance-of-149026

[29] L. Maier *u. a.*, „AixLib: an open-source Modelica library for compound building energy systems from component to district level with automated quality management“, *J. Build. Perform. Simul.*, Bd. 17, Nr. 2, S. 196–219, März 2024, doi: 10.1080/19401493.2023.2250521.

[30] H. Gadd und S. Werner, „Fault detection in district heating substations“, *Appl. Energy*, Bd. 157, S. 51–59, Nov. 2015, doi: 10.1016/j.apenergy.2015.07.061.